IOPscience iopscience.iop.org

Home Search Collections Journals About Contact us My IOPscience

Wide bandgap n-type and p-type semiconductor porous junction devices as photovoltaic cells

This content has been downloaded from IOPscience. Please scroll down to see the full text.

2011 J. Phys. D: Appl. Phys. 44 405103

(http://iopscience.iop.org/0022-3727/44/40/405103)

View the table of contents for this issue, or go to the journal homepage for more

Download details:

IP Address: 140.113.38.11
This content was downloaded on 24/04/2014 at 14:41

Please note that terms and conditions apply.

J. Phys. D: Appl. Phys. **44** (2011) 405103 (6pp) doi:10.1088/0022-3727/44/40/405103

Wide bandgap n-type and p-type semiconductor porous junction devices as photovoltaic cells

Yuan-Pai Lin[2], Yu-Chiang Chao[1], Hsin-Fei Meng[1], Hsiao-Wen Zan[3] and Sheng-Fu Horng[2]

[1] Institute of Physics, National Chiao Tung University, Hsinchu 300, Taiwan
[2] Institute of Electronics Engineering, National Tsing Hua University, Hsinchu 300, Taiwan
[3] Department of Photonics and Institute of Electro-Optical Engineering, National Chiao Tung University, Hsinchu 300, Taiwan

E-mail: yuchiangchao@gmail.com and meng@mail.nctu.edu.tw

Received 6 March 2011, in final form 18 August 2011
Published 14 September 2011
Online at stacks.iop.org/JPhysD/44/405103

Abstract
In junction absorber photovoltaics doped wide bandgap n-type and p-type semiconductors form a porous interpenetrating junction structure with a layer of low bandgap absorber at the interface. The doping concentration is high enough such that the junction depletion width is smaller than the pore size. The highly conductive neutral region then has a dentrite shape with fingers reaching the absorber to effectively collect the photo-carriers swept out by the junction electric field. With doping of 10^{19} cm^{-3} corresponding to a depletion width of 25 nm, pore size of 32 nm, absorber thickness close to exciton diffusion length of 17 nm, absorber bandgap of 1.4 eV and carrier mobility over 10^{-5} cm^2 V^{-1} s^{-1}, numerical calculation shows the power conversion efficiency is as high as 19.4%. It rises to 23% for a triplet exciton absorber.

(Some figures in this article are in colour only in the electronic version)

1. Introduction

Solar cells incorporating organic materials are interesting alternatives to conventional silicon solar cells because of their low production cost. Significant breakthroughs in solar cell performances have been achieved in recent years; however, their power conversion efficiency has to be enhanced further in order to improve their viability. Two exclusive transport channels, absorption at the channel interface and a high absorption cross section are, in general, the three prerequisites for an ideal solar cell. Photosynthesis in plants is an efficient way to harvest sunlight energy that fulfils these three prerequisites. However, so far, the three prerequisites have not been realized simultaneously in a single artificial photovoltaic device. In a dye-sensitized solar cell the absorbing dye molecules lie at the large interface between the porous metal oxide for electron transport and ionic liquid [1] or organic semiconductor [2] for hole transport. There is, however, no self-avoidance of the two transport channels. Moreover, the absorbance is low because there is only a monolayer of absorber [3]. The absorbance is improved in extremely thin absorber solar cells on highly structured substrates [4] and bulk hetero-junction solar cells [5, 6]; yet both have no self-avoidance in the channels either. Self-avoiding exclusive transport is realized in a p–n junction solar cell by the electrical field in the depletion region. The p–n junction solar cell, however, has a simple planar structure in sharp contrast to photosynthesis where the absorbers and channels are organized in a complex three-dimensional manner. In this work we propose and study theoretically a concept named junction absorber photovoltaics which combines simultaneously the three prerequisites. In this device a layer of absorber lies at the interface between a porous wide bandgap n-type semiconductor and a p-type semiconductor with appropriate doping. Figure 1(*a*) shows the random porous structure in reality which is modelled by a regular structure shown in figure 1(*b*). The red, green and blue regions represent the n-type semiconductor, absorber and p-type semiconductor, respectively. The porous p–n junction was used to have multiple absorption since the absorber is very thin. An

 © 2011 IOP Publishing Ltd Printed in the UK & the USA

enlarged regular structure model is shown in figure 1(*e*). The doping levels of n-type and p-type semiconductors are chosen such that the depletion region conformally overlaps the absorber and part of the semiconductor throughout the porous interface which means that the depletion width W is at least as thick as the thickness of the absorber d_a. At such doping levels, the depletion region does not extend much further so that the neutral region does not disappear. The neutral region has a three-dimensional dendritic geometry with fingers reaching the three-dimensionally distributed absorbers which are always only one depletion width away. The carriers generated inside the depletion region will then be swept by the strong junction electric field into the fingers and easily transported to the collecting electrode in the neutral dendrite due to the high conductivity. If the doping level is not sufficiently high, the depletion regions will merge and the neutral region fingers will disappear. As for the organic absorber, the excitons are generated immediately upon receiving the light because the binding energy is large which results from the small dielectric constant. There should be a conduction band offset between the absorber and the n-type semiconductor to overcome the exciton binding energy for dissociation exclusively at the interface of the intrinsic absorber and the n-type semiconductor. The optimal thickness of the absorber is about the exciton diffusion length which is far greater than the monolayer thickness. This thickness gives the greatest absorbance without sacrificing the exciton dissociation probability. This high absorbance significantly reduces the total solar cell thickness and the series resistance. There is therefore an intricate interplay between four length scales: the pore size, the depletion width, the absorber thickness and the exciton diffusion length.

This device concept can be realized as discussed below. For the porous n-type semiconductor, ZnO on ITO surface can be made. Al can be used to n-dope ZnO [7]. Random or ordered porous ZnO processed in solution can be used. The random porous structure can be made by sintering as in the case of dye-sensitized solar cells. The regular porous structure can be made by the sol–gel process with a polystyrene template [8, 9]. The polystyrene spheres were first deposited on the substrate as the template, then the ZnO precursor was deposited on the template to fill up the gaps between the polystyrene spheres. After annealing at a high temperature, the polystyrene spheres were vaporized and the ZnO precursor transformed into ZnO. Since ZnO is transparent, the light could pass through ZnO without any dramatic intensity attenuation. For the thin absorber, a low bandgap organic semiconductor, such as poly[2,6-(4,4-bis-(2-ethylhexyl)-4H-cyclopenta[2,1-b;3,4-b']dithiophene)-alt-4,7(2,1,3-benzothiadiazole)] (bandgap $\sim$ 1.4 eV) [10, 11] and thiophene-enriched fused-aromatic thienopyrazine (bandgap = 1.0–1.4 eV) [12] can be deposited by immersion in a solution of organic solvent. Chemical cross-linking by heating or ultraviolet irradiation can make them insoluble in the following steps. High bandgap organic semiconducting polymers such as poly[(9,9-dioctylfluorenyl-2,7-diyl)-co-(4,4′-(N-(4-sbutylphenyl))diphenylamine)] (TFB) [13] can be deposited by a solution in toluene to be used as the p-type semiconductor. The organic molecule F4-TCNQ

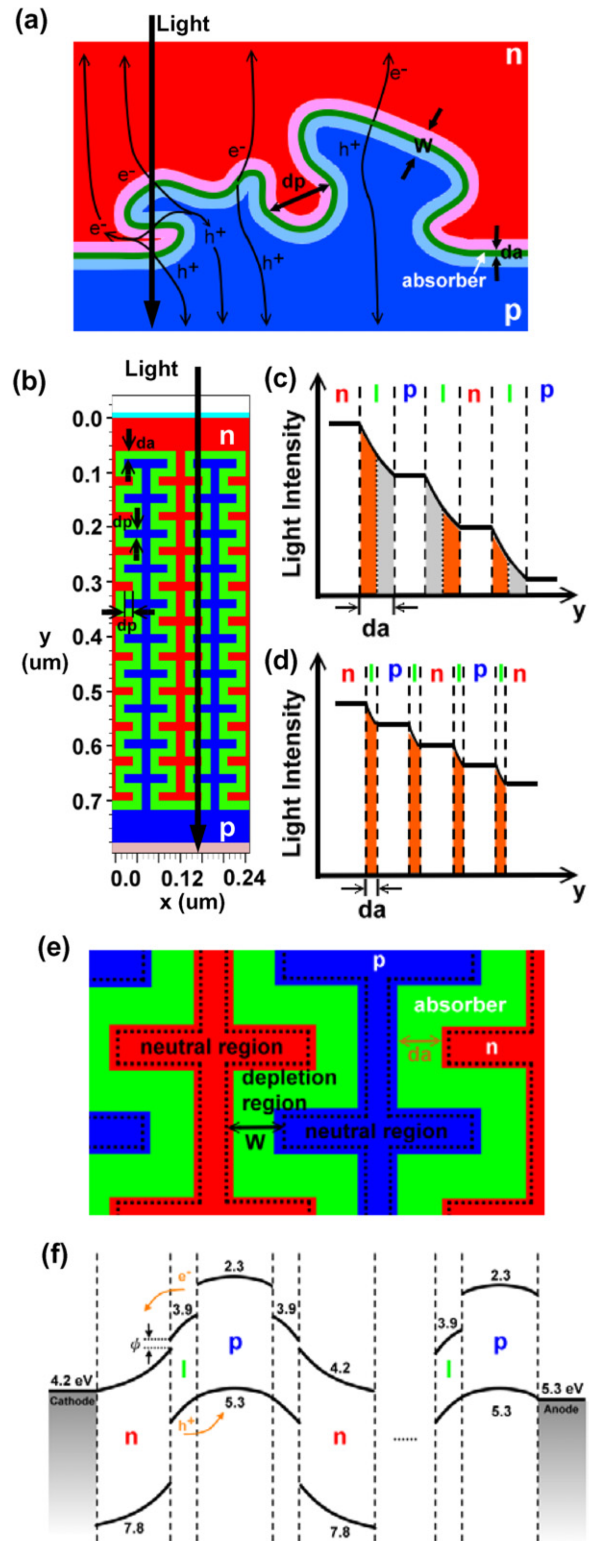

Figure 1. (*a*) Random porous structure in reality. W is the depletion width, d_a is the absorption thickness and d_p is the pore size. (*b*) Model structure. (*c*) Light intensity decay of a device with large d_a after multiple absorption. (*d*) Light intensity decay of a device with small d_a after multiple absorption. (*e*) Enlarged regular structure model. The depletion and neutral regions are separated by black dashed line. (*f*) Energy bands and work functions.

with a high electron affinity can be used to p-dope the polymer [14, 15]. Numerical calculations with practical physical parameters demonstrate that the power conversion efficiency is as high as 20%. This work is the first to place the absorber inside the depletion region along the porous surface of an extremely thin absorber solar cell. In addition, the influences of the doping concentrations of the n-type and p-type semiconductors are also investigated.

2. Model

The random porous structure in reality, depicted in figure 1(*a*), is modelled by a regular structure defined in figure 1(*b*). The structure is characterized by three geometry parameters: the pore size d_p, the absorption thickness d_a and the number of absorber layers n. The model structure in figure 1(*b*) is simulated by the Silvaco TCAD software. The energy bands and work functions are shown in figure 1(*f*). There is an electron barrier φ of 0.3 eV to prevent dark carriers from diffusing into the absorber region and recombining with photo-carriers [16, 17]. Density of state for both electrons and holes is assumed to be 10^{19} cm^{-3} [18]. The relative dielectric constant ε_r of the absorber and the p-type region is set to be 3.4 as in most organic materials [19]. ε_r is chosen as 9 taking ZnO as an example [20]. The boundary conditions are given by matching the sum of the thermionic-emission current and backflow current with the drift-diffusion current in the bulk at the metal-semiconductor interface. The incident photon flux is obtained by integrating the sunlight spectral density over photon energy above the absorber bandgap Eg. The absorption depth inside the absorber is taken as 200 nm [5]. Absorption is neglected in both n-type and p-type semiconductors because of their wide bandgaps. Excitons are generated in each absorber layer by light absorption as shown in figure 1(*c*). The probability $P_d(z)$ for an exciton to dissociate at the n–i interface is determined by the competition of two time constants: the time to diffuse to the interface and the decay lifetime. Their inverses are the rates k_d and k, respectively. The exciton diffusion length L_{ex} is $\sqrt{\tau D}$, where $\tau = 1/k$ and D is the exciton diffusion coefficient. z is the distance between the exciton generation position and the n–i interface. Expressed in terms of the exciton diffusion coefficient D, $P_d(z)$ is

$$p_d(z) = \frac{k_d}{k_d + k} = \frac{D/z^2}{(D/z^2) + k}.$$

For exictons generated at the p–i interface, the probability $P_d(d_a)$ is $L_{ex}^2/(L_{ex}^2 + d_a^2)$. Indeed the dissociation probability is nearly unity as d_a is much smaller than L_{ex}. The absorber thickness d_a, however, cannot be very thin otherwise the effective light absorption will be small and some light will penetrate the entire structure without being absorbed. The effect of d_a is illustrated in figures 1(*c*) and (*d*). For large d_a, the excitons generated outside the orange region will decay and are wasted. For small d_a, some light is not absorbed and wasted even after multiple penetrations through the absorber layers. $d_a \cong L_{ex}$ is therefore the optimal absorber thickness. The number of multiple absorption cannot be increased indefinitely to harvest the light because it will cause a large solar cell total

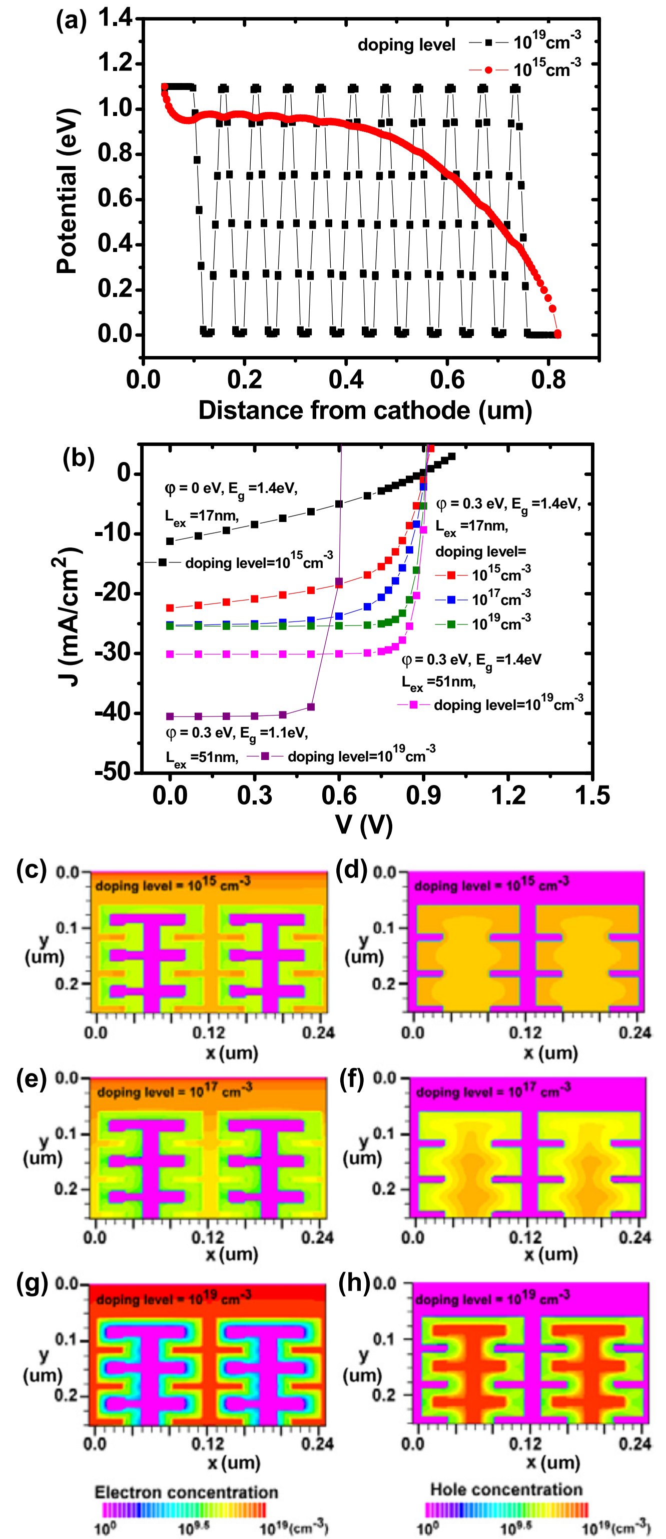

Figure 2. (*a*) Potential profile under the short-circuit condition. (*b*) Effect of doping on power conversion efficiency. Electron distribution as electron doping level is (*c*) 10^{15} cm^{-3}, (*e*) 10^{17} cm^{-3} and (*g*) 10^{19} cm^{-3}. Hole distribution as hole doping level is (*c*) 10^{15} cm^{-3}, (*e*) 10^{17} cm^{-3} and (*g*) 10^{19} cm^{-3}.

thickness and high transport resistance. In practice, the photon flux in each absorber layer is $\Phi(y) = \Phi(y_n)\exp[-(y - y_n)/\delta]$ where y is the vertical coordinate defined in figure 1(*b*) and y_n is the boundary of the nth absorber layer. Between the

Table 1. Summary of device performance with different electron barrier (ϕ), bandgap (E_g), exciton diffusion length (L_{ex}), hole mobility (μ_h), doping level and absorber thickness (d_a). Electron mobility (μ_e) is 10^{-1} cm^2 V^{-1} s^{-1}.

μ_h (cm^2 V^{-1} s^{-1})	Doping (cm^{-3})	d_a (nm)	J_{sc} (mA cm^{-2})	V_{oc} (V)	FF (%)	PCE (%)
$E_g = 1.4$ eV, $\varphi = 0.3$ eV, $L_{ex} = 17$ nm						
10^{-3}	10^{19}	10	23.1	0.91	81.7	17.2
10^{-3}	10^{19}	16	25.4	0.91	84.1	19.4
10^{-3}	10^{19}	20	23.9	0.91	83.4	18.1
10^{-3}	10^{17}	16	25.2	0.91	67.7	15.5
10^{-3}	10^{15}	16	22.4	0.91	58.1	11.8
10^{-4}	10^{19}	16	25.4	0.91	83.5	19.3
10^{-4}	10^{15}	16	20.4	0.91	45.9	8.5
10^{-5}	10^{19}	16	25.4	0.91	81.6	18.9
10^{-5}	10^{15}	16	13.5	0.91	18.8	2.3
$E_g = 1.4$ eV, $\varphi = 0.3$ eV, $L_{ex} = 51$ nm						
10^{-3}	10^{19}	16	30.1	0.91	84.2	23.1
$E_g = 1.1$ eV, $\varphi = 0.3$ eV, $L_{ex} = 51$ nm						
10^{-3}	10^{19}	16	40.5	0.61	80.1	19.8

absorber layers $\Phi(y)$ remains constant as shown in figures 1(*c*) and (*d*). The exciton generation rate is $g(y) = -\frac{d\Phi(y)}{dy}$. The total carrier generation in each absorber layer is the integration of dissociation probability P_d and the exciton generation rate g, which is $\int_{y_n}^{y_n+d_a} p_d(y-y_n)g(y)\,dy = (1/\delta)\Phi(y_n)\int_0^{d_a} p_d(z)e^{-z/\delta}\,dz$. We use the user-defined carrier generation rate in Silvaco TCAD such that the total carrier generation in each absorber layer is concentrated near the n–i interface where exciton dissociation actually occurs. Exciton diffusion coefficient D is 3×10^{-3} cm^2 s^{-1} [21]. The exciton decay lifetime τ is 1 ns [22, 23]. Exciton diffusion length $L_{ex} = \sqrt{\tau D}$ is 17 nm. The energy levels of the materials are shown in figure 1(*f*). The absorber bandgap is 1.4 eV unless otherwise specified.

3. Results and discussion

The doping levels N_A and N_D are equal and change from 10^{15} cm^{-3} to 10^{19} cm^{-3} in figure 2. The simulated depletion widths inside the n and p regions are slightly different but consistent with the theoretical relation for p–n junction without an intrinsic layer in between:

$$W_{n,p} = \left[\frac{2\varepsilon V_{bi}}{e}\left(\frac{N_{A,D}}{N_{D,A}(N_D + N_A)}\right)\right]^{1/2}.$$

The depletion regions do not merge if the pore size d_p is larger than both $2W_n$ and $2W_p$. The mobilities of the majority carrier are 10^{-1} cm^2 V^{-1} s^{-1} and 10^{-3} cm^2 V^{-1} s^{-1} in the n-type and p-type regions, respectively, while the mobilities of the minority carrier in the n-type and p-type regions are both 10^{-4} cm^2 V^{-1} s^{-1}. The potential profile under the short-circuit condition is plotted in figure 2(*a*) to examine whether the depletion regions merge. For a high doping level, the potential switches rapidly between 1.1 V and 0 V with a high field in the depletion regions and low field neutral regions in between, meaning the condition $d_p > 2W_n$ holds. The fingers of p-type and n-type regions extend well towards each other as shown by the carrier distribution in figures 2(*g*) and (*h*). The red part, which is the neutral region, has the highest carrier density. As expected, it has dentritic fingers reaching the absorber layer at the junction. On the other hand, for low doping levels such that $d_p < 2W_{n,p}$, the potential energy varies slowly from 1.1 V to 0 V with position as the depletion regions merge together. The fingers in the red neutral region disappear as shown in figures 2(*c*) and (*d*). Figure 2(*b*) shows the effect of doping on power conversion efficiency. As the doping level increases, the short-circuit current J_{sc} increases moderately but the fill factor grows remarkably, and the open-circuit voltage V_{oc} is fixed at around 0.9 V which is close to the electrode work function difference of 1.1 eV. At high doping levels where the fingers of p-type and n-type regions extend into each other, electrons and holes generated in the high-field depletion region are pushed away from each other, and then quickly extracted. Thus, the recombination in the absorber layer is highly reduced, resulting in a high fill factor and power conversion efficiency. On the other hand, for low doping levels where the fingers shrink and depletion regions merge, carrier extraction becomes difficult and the recombination in the absorber layer is severe, causing lower fill factor and efficiency. For exciton diffusion length L_{ex} of 17 nm the maximal efficiency is 19.4% for $N_a = 10^{19}$ cm^{-3}. The fill factor is as high as 84.1% because of the lack of recombination. Efficiency drops for lower doping levels. If the singlet excitonic level of the absorber is above the triplet excitonic level and if intersystem crossing is present, the exciton becomes spin triplet with much longer lifetime and diffusion length. Taking triplet L_{ex} as 51 nm the power efficiency is increased to 23.1%. Figure 2(*b*) also demonstrates that the electron barrier φ is necessary to block the dark carriers diffused from the electrode [24]. The results are summarized in table 1.

The effect of absorber thickness is shown in figure 3. As illustrated in figure 1(*c*), for large d_a, the photon absorption in the grey areas are wasted because the position is too far away from the n–i junction. For small d_a, there is no grey area, as shown in figure 1(*d*), but there is a high wasted residual light intensity after multiple absorption. Figure 3 shows that, as expected, the optimal absorber thickness 16 nm is close to the exciton diffusion length $L_{ex} = 17$ nm. The corresponding efficiency is 10% for $d_a = 5$ nm, 19.4% for $d_a = 16$ nm, and drops to 18.1% for $d_a = 20$ nm. With 21 multiple absorption, the total light path $n \times d_a$ is 336 nm

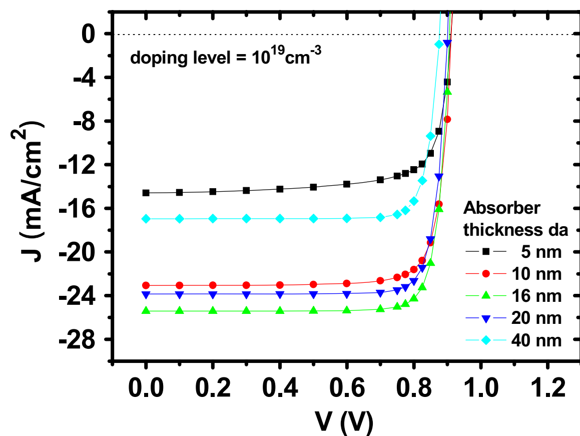

Figure 3. Influence of absorber thickness d_a on power conversion efficiency.

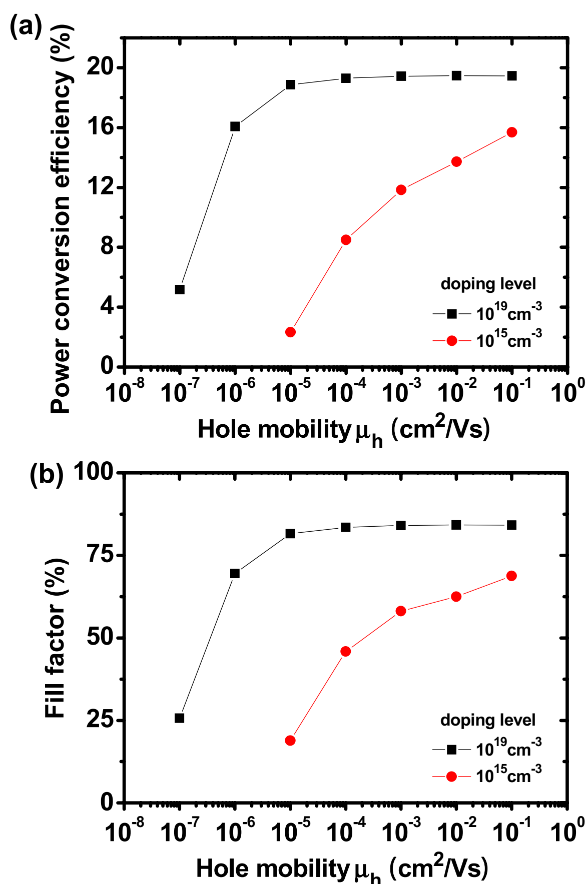

Figure 4. Effect of carrier mobility on (*a*) power conversion efficiency and (*b*) fill factor.

which is about 1.5 times of the absorption depth $\delta = 200$ nm to ensure nearly complete absorption. The total cell thickness is 640 nm with 10 repeat unit of 64 nm. The absorber thickness of 16 nm is more than ten times larger than the monolayer thickness in dye-sensitized solar cell. Consequently, the total cell thickness is less than 1/10 of the dye-sensitized solar cell thickness of several micrometres. The reduced cell thickness has the great advantages of low series resistance and less recombination in the collection path. Mobility effect is shown in figure 4 where μ_e is fixed at 0.1 $cm^2 V^{-1} s^{-1}$. For low doping of $N_a = 10^{15} cm^{-3}$, the efficiency and fill factor reach the maximum only for hole mobility μ_h over 0.1 $cm^2 V^{-1} s^{-1}$. Remarkably, for high doping of $10^{19} cm^{-3}$, the fill factor and efficiency rapidly increase and saturate at 84% and 19% as the hole mobility is above a mere $10^{-5} cm^2 V^{-1} s^{-1}$. This is because the high carrier density in the neutral region supports a negligible series resistance even for low carrier mobility typical for organic semiconductors, implying high mobility is not required.

4. Conclusions

In conclusion, a numerical calculation is performed to verify the concept of junction absorber solar cells inspired by and similar to photosynthesis, where a layer of intrinsic low bandgap absorber lies at the porous p–n junction interface of doped wide bandgap semiconductors. In practice, the dendritic junction can be realized between n-doped metal oxide semiconductor and p-doped conjugated polymers. With intriguing physics, high efficiency, and easy solution fabrication the junction absorber photovoltaics open a new paradigm to solve energy challenges.

Acknowledgment

This work is supported by the National Science Council of Taiwan under Contract No NSC98-2628-M-009-001.

References

[1] O'Regan B and Grätzel M 1991 *Nature* **353** 737
[2] Jiang K J, Manseki K, Yu Y H, Masaki N, Suzuki K, Song Y l and Yanagida S 2009 *Adv. Funct. Mater.* **19** 2481
[3] Grätzel M 2001 *Nature* **414** 338
[4] Ernst K, Belaidi A and Könenkamp R 2003 *Semicond. Sci. Technol.* **18** 475
[5] Li G, Shrotriya V, Huang J, Yao Y, Moriarty T, Emery K and Yang Y 2005 *Nature Mater.* **4** 864
[6] Hoppe H, Niggemann M, Winder C, Kraut J, Hiesgen R, Hinsch A, Meissner D and Sariciftci N S 2004 *Adv. Func. Mater.* **14** 1005
[7] Xu Z Q, Deng H, Li Y and Cheng H 2006 *Mater. Sci. Semicond. Process.* **9** 132
[8] Liu C C, Li J H, Chang C C, Chao Y C, Meng H F, Horng S F, Hung C H and Meng T C 2009 *J. Phys. D: Appl. Phys.* **42** 155105
[9] Orilall M C, Abrams N M, Lee J, DiSalvo F J and Wiesner U 2008 *J. Am. Chem. Soc.* **130** 8882
[10] Soci C, Hwang I-W, Moses D, Zhu Z, Waller D, Gaudiana R, Brabec C J and Heeger A J 2007 *Adv. Funct. Mater.* **17** 632
[11] Morana M, Wegscheider M, Bonanni A, Kopidakis N, Shaheen S, Scharber M, Zhu Z, Waller D, Gaudiana R and Brabec C 2008 *Adv. Funct. Mater.* **18** 1757
[12] Mondal R *et al* 2010 *J. Mater. Chem.* **20** 5823
[13] Kim J S, Friend R H, Grizzi I and Burroughes J H 2005 *Appl. Phys. Lett.* **87** 023506
[14] Yim K H, Whiting G L, Murphy C E, Halls J J M, Burroughes J H, Friend R H and Kim J S 2008 *Adv. Mater.* **20** 3319
[15] Zhang Y, de Boer B and Blom P W M 2009 *Adv. Funct. Mater.* **19** 1901

[16] Wang Y X, Tseng S R, Meng H F, Lee K C, Liu C H and Horng S F 2008 *Appl. Phys. Lett.* **93** 133501
[17] Brabec C J, Winder C, Sariciftci N S, Hummelen J C, Dhanabalan A, van Hal P A and Janssen R A J 2002 *Adv. Funct. Mater.* **12** 709
[18] Koster L J A, Smits E C P, Mihailetchi V D and Blom P W M 2005 *Phys. Rev.* B **72** 085205
[19] Koster L J A, Mihailetchi V D and Blom P W M 2006 *Appl. Phys. Lett.* **88** 093511
[20] Sze S M 2007 *Physics of Semiconductor Devices* 3rd edn (New York: Wiley)
[21] Lewis A J, Ruseckas A, Gaudin O P M, Webster G R, Burn P L and Samuel I D W 2006 *Org. Electron.* **7** 452
[22] Greenham N C, Samuel I D W, Hayes G R, Phillips R T, Kessener Y A R R, Moratti S C, Holmes A B and Friend R H 1995 *Chem. Phys. Lett.* **241** 89
[23] Yan M, Rothberg L J, Papadimitrakopoulos F, Galvin M E and Miller T M 1994 *Phys. Rev. Lett.* **73** 744
[24] Cunningham P D and Hayden L M 2008 *J. Phys. Chem.* C **112** 7928